Int. J. Advanced Design and Manufacturing Technology, 2024, Vol. 17, No. 3, pp. 49-64

DOI: 10.30486/ADMT.2024.873778 *ISSN: 2252-0406* *https://admt.isfahan.iau.ir*

Friction-Adaptive Integrated Position Control for Vehicles on Curved Paths

Hadi Sazgar *
Department of Mechanical Engineering,
Iranian Research Organization for Science and Technology (IROST), Iran
E-mail: sazgar@irost.ir
*Corresponding author

Ali Keymasi-Khalaji
Department of Mechanical Engineering, Faculty of Engineering,
Kharazmi University, Iran
E-mail: keymasi@khu.ac.ir

Received: 6 January 2024, Revised: 12 June 2024, Accepted: 4 August 2024

Abstract: In critical manoeuvres where the maximum tire-road friction capacity is used, the vehicle's dynamic behaviour is highly nonlinear, and there are strong couplings between longitudinal and lateral dynamics. If the tire-road friction conditions change suddenly during these manoeuvres, the vehicle control will be very complicated. The innovation of this research is a control algorithm to manage vehicles on a curved path with sudden tire-road friction change. The main advantage of the proposed controller is that it is robust to the change of the friction coefficient and other unmodeled uncertainties and ensures vehicle stability with low computational volume. The evaluation of the proposed adaptive controller has been done using the full vehicle model in CarSim software and by defining three different manoeuvres, moving at a constant speed on a curved road, lane-change, and lane-change with braking. Also, in the obtained results, the noise of the yaw speed signals and longitudinal and lateral accelerations are considered. The estimation of the longitudinal and lateral velocities is also done using these data. The obtained results showed that the proposed integrated control can manage the highly nonlinear dynamics of the vehicle in the existence of a sudden and significant change in the friction coefficient.

Keywords: Integrated Longitudinal and Lateral Control, Kinetic Control, Kinematic Control, Nonlinear Tire, Seven Degrees of Freedom Dynamic Model, Tire-Road Friction Estimation,

Biographical notes: Hadi Sazgar earned his BSc degree from Shahid Bahonar University of Kerman (SBUK), Kerman, Iran, in 2007, followed by his MSc and PhD in Mechanical Engineering from K. N. Toosi University of Technology (KNTU), Tehran, in 2009 and 2019, respectively. He is an assistant professor in the Mechanical Engineering Department at the Iranian Research Organization for Science and Technology (IROST) in Tehran. His research interests focus on the modeling and control of mechanical systems, vehicle dynamic control, and advanced driver assistance systems (ADAS). **Ali Keymasi-Khalaji** received his BSc from Iran University of Science and Technology (IUST), Tehran, Iran, in 2007, and his MSc and PhD in Mechanical Engineering from K. N. Toosi University of Technology (KNTU), Tehran, in 2009 and 2014 respectively. He has been an associate professor with the Mechanical Engineering Department at Kharazmi University (KHU) in Tehran since 2015. His research interests include modeling and control of mechanical systems, nonlinear control, and adaptive and robust control with applications to mobile robotic systems and mechatronics.

Research paper

1 INTRODUCTION

Autonomous driving started in the 1980s [1-2] and has developed and progressed significantly over the past few decades [3]. Automatic driving can save time and reduce air pollution by reducing traffic. In addition, self-driving vehicles can significantly increase the comfort and safety. Based on accident statistics and the proportion of accidents caused by human error, there is a growing need for self-driving cars. The World Health Organization states that more than 1.35 million people die, and 20 to 50 million people are injured due to annual accidents worldwide. Economic studies also show that the costs caused by accidents are more than 3% of the gross domestic product of the countries [4]. A study by the National Highway Traffic Safety Administration (NHTSA) in 2015 shows that human error was effective in about 94 percent of all car accidents [5].

The self-driving car has different parts, one of the most important of which is the control algorithm. The control section must perform the path tracking with the desired accuracy and also ensure vehicle stability. In a critical maneuver in which the longitudinal and lateral movements are performed simultaneously, the tire is in its saturated range. During the manoeuvre, the tire-road friction conditions also change. Due to uncertainties and very strong couplings between longitudinal and lateral dynamics in several levels of dynamics, kinematics, and tire forces, the problem of path following and maintaining the stability of the vehicle in a critical manoeuvre will be very challenging and complex.

Literature review: So far, various control approaches have been proposed to solve this problem. One of the important manoeuvres in which longitudinal and lateral movements are performed at the same time is the lane change maneuverer. In [6-7], a review of the methods presented in the field of lane change control has been done. Depending on the desired manoeuvre, different controllers can be used. For simple manoeuvres where tire slip is negligible, a kinematic model can be used, and a controller can be designed for that [8-10]. Assuming that the slip of the tires is small, the relationship between force and slip is linear and it will be logical to use the linear dynamic model. In some references, the control algorithm has been studied based on a linear dynamic model [11-18]. One of the very important manoeuvres that play a role in reducing accidents is the collision avoidance manoeuvre. Numerous researchers have studied the problem of longitudinal and lateral integrated control with an emphasis on collision avoidance [19-23]. Model predictive control has been used many times in various areas of vehicle control due to its high capability in managing multi-objective constrained systems with uncertainty [24-26]. In some cases, predictive control has been used along with other methods. In [27], the direct Lyapunov approach has been used for longitudinal velocity control and nonlinear predictive control (NMPC) for lateral control. Despite having many capabilities, predictive control also brings challenges. By growing the model order, nonlinear terms, and constraints, the computational cost increases, and the possibility of getting stuck in the local minimum while doing the optimization problem increases.

In [28], a comprehensive approach that combines planning and control mechanisms to enhance the quality of trajectories produced by intelligent vehicles is introduced. The trajectory planning component is engineered using the principles of the Iterative Linear Quadratic Regulator (ILQR), which incorporates the vehicle's nonlinear dynamics to optimize trajectory planning. In [29], a combined H∞ control approach is designed to enhance both the path-following capabilities and the lateral stability of autonomous in-wheel-motor-driven electric vehicles (AIEVs) is presented.

Motivation and innovation: The prior surveys show that valuable research has been conducted in this field. However, the problem of integrated longitudinal and lateral control of the vehicle in critical manoeuvres still needs more investigation. The primary objective of this work is to develop an adaptive control algorithm capable of providing integrated longitudinal and lateral control for highly nonlinear vehicle dynamics, while being robust to sudden changes in the friction coefficient and other uncertainties. A key goal is also to enable the control system to effectively follow curved paths, in addition to managing linear manoeuvres, by separating the control architecture. These objectives are motivated by the need to enhance vehicle safety and performance in challenging driving conditions where the available tire-road friction can vary unexpectedly. In [30-31], the motion control and integrated longitudinal and lateral control in the critical lane change manoeuvre on the highways have been done. To manage the variations of tire and road friction conditions, an adaptive control algorithm is proposed in [32]. This control algorithm uses the sliding mode approach, and by considering the nonlinear tire dynamics, it updates the tire forces in the control law by changing the friction conditions of the tire and the road. Despite having many advantages such as low computational cost, stability, and high tracking accuracy, this controller also has a fundamental limitation.

This control algorithm is only used for lane change manoeuvres on the highways, where the lateral position variation is small compared to the longitudinal position. This article proposes a new control algorithm for critical manoeuvres to overcome this limitation. This algorithm can be used for the integrated longitudinal and lateral dynamics control of the vehicle on all roads (straight and curved roads). The accuracy of trajectory tracking of this algorithm is very high, and it also guarantees vehicle stability. This controller also can adapt to variations in

the tire-road friction conditions. This algorithm is robust to unmodeled uncertainties and parameter changes, and it will be helpful for manoeuvres where the vehicle dynamics are highly nonlinear and the tire capacity is in the saturated range. The details related to the design of the integrated controller, as well as the estimation algorithm of tire forces and friction coefficient, will be presented in sections 3 and 4, respectively.

2 VEHICLE DYNAMIC MODEL

In high-speed manoeuvres, it is possible to analyse the real behaviour of the vehicle only with a nonlinear dynamic model with many degrees of freedom. On the other hand, due to unmodeled uncertainties and the unknown value of the parameters, it is practically impossible to design a model-based controller based on complex dynamic models with high degrees of freedom. Considering these considerations, in this research, 7 degrees of freedom model, including three degrees for movements in the yaw plane (x, y and ψ) and four degrees of freedom for four wheels, are used. The overview of this model is shown in "Fig. 1". This model considers longitudinal and lateral load transfer caused by longitudinal and lateral accelerations. The simulations performed on a complete vehicle model show that the design of the controller based on the 7-degree-of-freedom model $(x, y, \psi, \omega_{f,l}, \omega_{f,r}, \omega_{r,r}, \omega_{r,l})$ was practical and appropriate (Section 5).

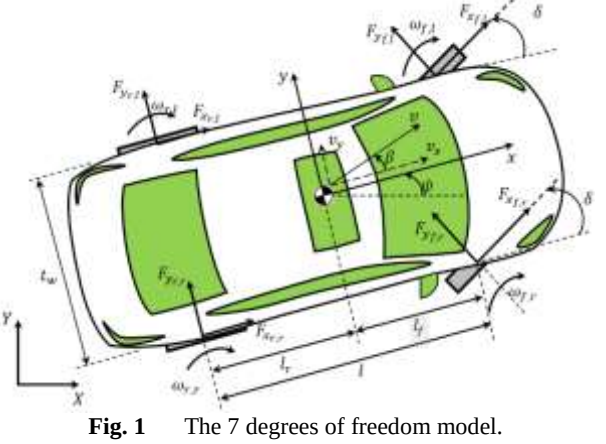

Fig. 1 The 7 degrees of freedom model.

In "Fig. 1", $X-Y$ are the inertial coordinate axes, and x-y are the local coordinate axes connected to the centre of mass (CG). Subscripts f and r refer to the front axle and rear axle of the vehicle. Also, the pairs (f,l), (f,r), (r,r), and (r,l)refer to the left front, right front, right rear, and left rear tires, respectively. F_x and F_y represent the longitudinal and lateral forces of the tire, respectively. The symbol ω also indicates the rotation around the wheel spinning axis. The longitudinal and lateral speeds at the CG are measured in local coordinates and are introduced by variables v, v_x and v_y, respectively. δ, ψ, and β stand for the front wheel steering angle, vehicle yaw angle, and vehicle side-slip angle, respectively. The description and values of dynamic model parameters are presented in "Table 1". The values of this table are extracted from D-Class Sedan vehicle in the CarSim software.

In the following, the details of other parts of the dynamic model are stated.

Table 1 Vehicle dynamic model parameters [30]

Parameter	Value	Unit	Description
m	1530	kg	The total mass of the vehicle
I_z	2315	kgm^2	Vehicle yaw moment of inertia
l_f	1.11	m	Front axle CG distance
l_r	1.67	m	Rear-axle CG distance
t_w	1.55	m	Track width
h_{CG}	0.52	m	Height of CG
C_d	0.3	---	Aerodynamic drag coefficient
k_b	700	(N. m) /MPa	Braking gain
τ_b	0.06	---	Brake actuator time constant
τ_{bd}	31	msec	Brake delay
η_d	0.85	---	Driveline efficiency
k_{diff}	4.1	---	Driveline gain
r_w	0.325	m	Effective wheel radius
I_w	0.9	kg. m^2	Wheel's moment of inertia
f_r	0.015	---	Rolling resistance coefficient

2.1. Vehicle Motion Equations [33]

$$\begin{aligned}\left(\dot{v}_x - v_y\dot{\psi}\right) = \Big[&\left(F_{x_{f,l}} + F_{x_{f,r}}\right)\cos\delta \\ &- \left(F_{y_{f,l}} + F_{y_{f,r}}\right)\sin\delta \\ &+ \left(F_{x_{r,l}} + F_{x_{r,r}}\right) - F_{aero}\Big]\end{aligned} \tag{1}$$

$$\begin{aligned}m\left(\dot{v}_y + v_x\dot{\psi}\right) = \Big[&\left(F_{x_{f,l}} + F_{x_{f,r}}\right)\sin\delta \\ &+ \left(F_{y_{f,l}} + F_{y_{f,r}}\right)\cos\delta \\ &+ \left(F_{y_{r,l}} + F_{y_{r,r}}\right)\Big]\end{aligned} \tag{2}$$

$$\begin{aligned}I_z\ddot{\psi} = l_f\Big[&\left(F_{x_{f,l}} + F_{x_{f,r}}\right)\sin\delta + \left(F_{y_{f,l}} + F_{y_{f,r}}\right)\cos\delta\Big] \\ &- l_r\left(F_{y_{r,l}} + F_{y_{r,r}}\right)\end{aligned} \tag{3}$$

Where, $\dot{\psi}$ and $\ddot{\psi}$ are the rotational velocity and

acceleration of the vehicle, respectively. F_{aero} also represents the aerodynamic force applied to the front surface of the vehicle defined by "Eq. (4)", [33]:

$$F_{aero} = \frac{1}{2}\rho C_d A_F (v_x + v_{wind})^2 \quad (4)$$

Where, ρ is the air density and v_{wind} is the wind speed. A_F also represents the effective front surface of the vehicle and is equal to $1.6 + 0.00056(m - 765)$, [33].

2.2. Tire Model

For the behaviour of the tire model to be close to the real behaviour, complex and accurate models should be used [33-35]. Accurate models have many parameters that must be identified. Identifying these parameters will be a major challenge considering the variations in tire and road conditions. Even if these parameters are identified, due to the accumulation of dynamic modelling errors and identification errors, the resulting tire and road friction model may significantly differ from the actual friction behaviour. In addition, the selected model for controlling the base model should be as simple as possible. Fortunately, if robust control approaches are used, it can be ensured that the unmodeled uncertainties of the tire will be well covered. Considering these considerations, based on the friction circle, a version of Pacejka's tire model, which has been used for control applications in this field [36-37], will be used [38]. Of course, for integrated control with friction estimation, this tire model will be used with modifications that will be explained in section 4.

$$F_{\gamma_{\tau,\varepsilon}} = \frac{\sigma_{\kappa_{\tau,\varepsilon}}}{\sigma_{\tau,\varepsilon}} \mu_{\tau,\varepsilon} F_{z_{\tau,\varepsilon}}, \quad \kappa \in \{x, y\}, \quad \tau \in \{f, r\}, \quad \varepsilon \in \{l, r\} \quad (5)$$

In this Equation, $F_{z_{\tau,\varepsilon}}$ represents the vertical load of each tire and $\mu_{\gamma_{\tau,\varepsilon}}$ stands for the longitudinal or lateral tire-road friction coefficient. $\sigma_{\tau,\varepsilon}$ also represents the total tire slip, which is a function of the longitudinal slip ($\sigma_{x_{\tau,\varepsilon}}$) and lateral slip ($\sigma_{y_{\tau,\varepsilon}}$) of the tire ($\sigma_{\tau,\varepsilon} = \sqrt{\left(\sigma_{x_{\tau,\varepsilon}}\right)^2 + \left(\sigma_{y_{\tau,\varepsilon}}\right)^2}$) [38]. By considering the effect of load transfer caused by longitudinal and lateral accelerations using D'Alembert's principle, the vertical force of tires can be approximated with the following relationship. It must be recognized that the effect of vehicle suspension has been ignored.

$$F_{z_{f,l}} = m\left[\frac{g l_r - a_x h_{CG} - F_{aero} h_{aero}/m}{2l} - \frac{l_r}{l}\frac{h_{CG}}{t_w} a_y\right] \quad (6)$$

$$F_{z_{f,r}} = m\left[\frac{g l_r - a_x h_{CG} - F_{aero} h_{aero}/m}{2l} + \frac{l_r}{l}\frac{h_{CG}}{t_w} a_y\right] \quad (7)$$

$$F_{z_{r,l}} = m\left[\frac{g l_f + a_x h_{CG} + F_{aero} h_{aero}/m}{2l} - \frac{l_f}{l}\frac{h_{CG}}{t_w} a_y\right] \quad (8)$$

$$F_{z_{r,r}} = m\left[\frac{g l_f + a_x h_{CG} + F_{aero} h_{aero}/m}{2l} + \frac{l_f}{l}\frac{h_{CG}}{t_w} a_y\right] \quad (9)$$

2.2.1. Longitudinal Slip Ratio [38]

$$\sigma_{x_{\tau,\varepsilon}} = \frac{v_{rw_{\tau,\varepsilon}} - v_{cw_{\tau,\varepsilon}}}{\max\left(v_{rw_{\tau,\varepsilon}}, v_{cw_{\tau,\varepsilon}}\right)}, \tau \in \{f, r\}, \varepsilon \in \{l, r\} \quad (10)$$

In the above Equations, $v_{cw_{\tau,\varepsilon}}$ is the longitudinal velocity of the tire contact point with the road surface and $v_{rw_{\tau,\varepsilon}}$ is the longitudinal velocity equivalent to the rotation of the wheel [34].

2.2.2. Tire Slip Angle [33]

$$\sigma_{f,l} = \sigma_{f,r} = \delta - \arctan\left(\frac{v_y + \dot{\psi} l_f}{v_x}\right) \quad (11)$$

$$\sigma_{r,l} = \sigma_{r,r} = -\arctan\left(\frac{v_y - \dot{\psi} l_r}{v_x}\right) \quad (12)$$

2.3. Wheel Dynamics

The wheel motion Equation establishes the relationship between the longitudinal force and the traction and braking torques [33].

$$I_w \dot{\omega}_{\tau,\varepsilon} = -F_{x_{\tau,\varepsilon}} . r_w + \left(T_{d_{\tau,\varepsilon}} - T_{b_{\tau,\varepsilon}}\right) - f_r F_{z_{\tau,\varepsilon}} r_w, \quad \tau \in \{f, r\}, \quad \varepsilon \in \{l, r\} \quad (13)$$

Where, $\dot{\omega}$ is the angular acceleration of the wheel, $T_{d_{\tau,\varepsilon}}$ is the traction torque, $T_{b_{\tau,\varepsilon}}$ is the braking torque applied to the wheel.It is assumed that the torque applied to the left and right wheels of the front axle are equal to each other. This assumption is also valid for the wheels of the rear axle. It must be recognized that the traction torque is applied only to the front wheels. It is also assumed that in the braking mode, the distribution ratio of the rear-to-front braking torques is equal to γ. The parameter γ is determined using the pressure distribution valve of the hydraulic system [33]. Therefore, the torques applied to the wheels can be defined as "Eq. (14) and Eq. (15)".

$$T_{d_{f,l}} = T_{d_{f,r}} = \frac{T_d}{2}, \quad T_{d_{r,l}} = T_{d_{r,r}} = 0 \tag{14}$$

$$T_{b_{\tau,l}} = T_{b_{\tau,r}} = \frac{T_{b_\tau}}{2}, \quad \tau \in \{f, r\} \tag{15}$$

It should be noted that T_d and T_b represent the sum of traction and braking torques applied to the wheels, respectively.

2.4. Power Train Model

It can be presumed that the torque converter is completely locked in high-speed maneuvers. So, the relationship between the engine torque (T_e) and the total traction torque (T_d) can be expressed as "Eq. (16)", [33].

$$T_e = \frac{T_d}{\eta_d k_{diff} n_g} \tag{10}$$

Where, n_g is the gear transmission ratio.

Also, the throttle opening percentage is a function of the engine's net torque (T_e) and its rotation speed (ω_e). This function is available as a lookup table ($\alpha_{th} = f(\omega_e, T_e)$).

2.5. Brake Dynamics

The relationship between the brake torque and the pressure in the main cylinder (P_b) can be approximately expressed by "Eq. (17)", [39]:

$$\frac{T_b(s)}{P_b(s)} = \frac{k_b e^{-\tau_{bd} s}}{\tau_b s + 1} \tag{17}$$

3 LONGITUDINAL AND LATERAL INTEGRATED CONTROL

The proposed control method is a robust control approach that can also be used for curved roads. This controller includes two kinematic and dynamic parts. Separating the system control into two kinematic and dynamic parts makes it possible to control the system position variables. Therefore, in this way, it becomes possible to follow curved paths. The general structure of the controller is such that first, in the kinematics section, the desired longitudinal and lateral velocity is determined based on the tracking longitudinal and lateral position errors. Then, in the dynamic control, appropriate inputs are calculated to reach the desired velocities required in the kinematic control, considering the vehicle dynamics.

3.1. Kinematic Control

The desired position vector is $p_R = \begin{bmatrix} X_R \\ Y_R \end{bmatrix}$, which represents the desired longitudinal and lateral positions, respectively. Also, the vehicle position vector is defined as $p = \begin{bmatrix} X \\ Y \end{bmatrix}$ ("Fig. 2"). The error vector, e, is also expressed as the difference between the desired position vector and the vehicle position vector.

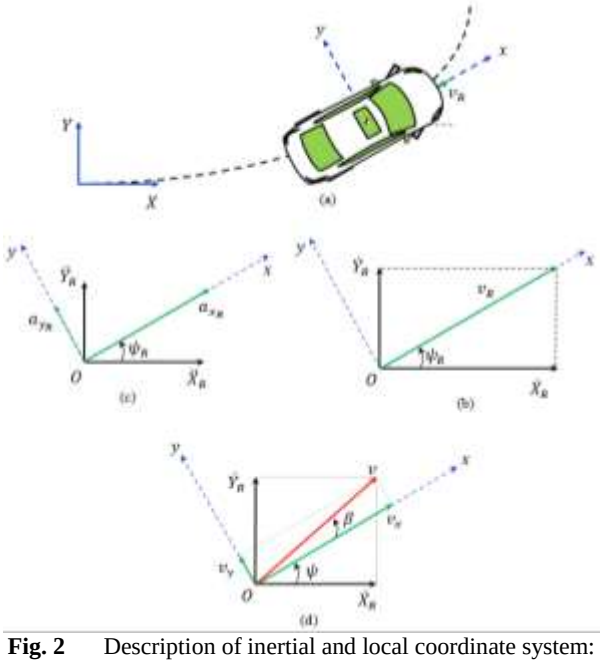

Fig. 2 Description of inertial and local coordinate system: (a): positions, (b): velocities (β=0), (c): accelerations, and (d): velocities (β≠0).

$$e = p_R - p = \begin{bmatrix} X_R - X \\ Y_R - Y \end{bmatrix}$$

The error dynamics for kinematic control is also expressed as:

$$\dot{e} + K_c e + K_{i,c} \int_0^t e \, dt = 0 \tag{18}$$

Where, K_c and $K_{i,c}$ are positive definite control gain matrixes. According to "Fig. 2" and assuming $R = \begin{bmatrix} \cos\psi & -\sin\psi \\ \sin\psi & \cos\psi \end{bmatrix}$, the velocity components in the inertial coordinates can be related to the components of the local coordinates as:

$$\begin{bmatrix} \dot{X} \\ \dot{Y} \end{bmatrix} = R \begin{bmatrix} v_x \\ v_y \end{bmatrix} \tag{19}$$

By combining "Eq. (18) and Eq. (19)", the desired velocity vector v_c can be written as:

$$v_c = \begin{bmatrix} v_{x_c} \\ v_{y_c} \end{bmatrix} = R^{-1} \left[\dot{p}_R + K_c e + K_{i,c} \int_0^t e \, dt \right] \tag{20}$$

3.2. Dynamicic Control

The goal of dynamic control is to make v_x and v_y tend to values v_{x_c} and v_{y_c} respectively. Therefore, the error of longitudinal and lateral velocities can be expressed as:

$$e_{v_x} = v_{x_c} - v_x \tag{21}$$

$$e_{v_y} = v_{y_c} - v_y \tag{22}$$

The error dynamics of longitudinal and lateral velocities can be defined as:

$$\dot{e}_{v_x} + K_{v_x} e_{v_x} + K_{i,v_x} \int_0^t e_{v_x}\, dt = 0 \tag{23}$$

$$\dot{e}_{v_y} + K_{v_y} e_{v_y i} + K_{i,v_y} \int_0^t e_{v_y}\, dt = 0 \tag{24}$$

Where K_{v_x}, K_{i,v_x}, K_{v_y} and K_{i,v_y} are positive definite control gain matrixes.

3.2.1. Longitudinal Control

Equation (23) can be used to calculate the longitudinal control input (throttle opening rate or brake cylinder pressure). By simplifying, we have:

$$\dot{v}_x = \dot{v}_{x_c} + K_{v_x} e_{v_x} + K_{i,v_x} \int_0^t e_{v_x}\, dt \tag{25}$$

On the other hand, by combining the Equation of longitudinal motion and wheel dynamics ("Eq. (1) and Eq. (13)"), $\dot{v}_x$ can be defined as:

$$\dot{v}_x = \frac{1}{m}\left[\frac{T_f - f_r r_w F_{z_f} - I_w\left(\dot{\omega}_{f,l} + \dot{\omega}_{f,r}\right)}{r_w}\cos\delta + \left(\frac{T_r - f_r r_w F_{z_r} - I_w\left(\dot{\omega}_{r,l} + \dot{\omega}_{r,r}\right)}{r_w}\right) - F_{y_f}\sin\delta - F_{aero}\right] + v_y\dot{\psi} \tag{26}$$

By setting the right side of "Eq. (25) and Eq. (26)" equal, the total torque applied to the front and rear wheels can be calculated as:

$$\begin{aligned} T_f\cos\delta + T_r = mr_w\Bigg(&\dot{v}_{x_c} + K_{v_x} e_{v_x} \\ &+ K_{i,v_x}\int_0^t e_{v_x}\, dt + v_y\dot{\psi}\Bigg) \\ &+ r_w\left(F_{y_f}\sin\delta + F_{aero}\right) \\ &+ I_w\left(\left[\dot{\omega}_{f,l} + \dot{\omega}_{f,r}\right]\cos\delta + \dot{\omega}_{r,l} + \dot{\omega}_{r,r}\right) \\ &+ r_w\left[f_r F_{z_f}\cos\delta + f_r F_{z_r}\right] \end{aligned} \tag{27}$$

The dynamics of the brake system and the power train are different, and each has its inputs. So, in the following steps, extracting the control input for each one is described separately.

3.2.1.1. Braking Mode

In braking mode, the ratio of the braking torque of the rear wheels to the front is assumed to be γ. In addition, the torque applied to the left and right wheels is the same in each of the axles. According to these assumptions and "Eq. (27)", the braking torque applied to each can be expressed by:

$$\begin{aligned} T_b = 1/(\cos\delta + \gamma)\Bigg[mr_w\Bigg(&\dot{v}_{x_c} + K_{v_x} e_{v_x} \\ &+ K_{i,v_x}\int_0^t e_{v_x}\, dt + v_y\dot{\psi}\Bigg) \\ &+ r_w\left(F_{y_f}\sin\delta + F_{aero}\right) \\ &+ I_w\left(\left[\dot{\omega}_{f,l} + \dot{\omega}_{f,r}\right]\cos\delta + \dot{\omega}_{r,l} + \dot{\omega}_{r,r}\right) + r_w\left(f_r F_{z_f}\cos\delta + f_r F_{z_r}\right)\Bigg] \end{aligned} \tag{28}$$

By determining the total braking torque, the brake cylinder pressure can be determined using "Eq. (17)".

3.2.1.2. Traction Mode

As mentioned, torque is not applied to the rear wheels in traction mode. According to "Eq. (16) and Eq. (27)", the required engine torque can be expressed as:

$$\begin{aligned} T_b = 1/\left(\eta_d k_{diff} n_g\cos\delta\right)\Bigg[mr_w\Bigg(&\dot{v}_{x_c} + K_{v_x} e_{v_x} \\ &+ K_{i,v_x}\int_0^t e_{v_x}\, dt + v_y\dot{\psi}\Bigg) \\ &+ r_w\left(F_{y_f}\sin\delta + F_{aero}\right) \\ &+ I_w\left(\left[\dot{\omega}_{f,l} + \dot{\omega}_{f,r}\right]\cos\delta + \dot{\omega}_{r,l} + \dot{\omega}_{r,r}\right) + r_w\left(f_r F_{z_f}\cos\delta + f_r F_{z_r}\right)\Bigg] \end{aligned} \tag{29}$$

The throttle opening percentage can be determined by determining the engine torque and the engine speed.

3.2.2. Lateral Control

First, we multiply both sides of "Eq. (2)" by l_r and add the resulting Equation with Equation (3).

$$\begin{aligned} ml_r\left(\dot{v}_y + v_x\dot{\psi}\right) + I_z\ddot{\psi} \\ = l\left[\left(F_{x_{f,l}} + F_{x_{f,r}}\right)\sin\delta + \left(F_{y_{f,l}} + F_{y_{f,r}}\right)\cos\delta\right] \end{aligned} \tag{30}$$

By combining "Eq. (5), Eq. (11), and Eq. (30)", $\dot{v}_y$ can be defined as "Eq. (31)".

$$\dot{v}_y = \frac{l}{ml_r}\Bigg[F_{x_f}\sin\delta + b\left(\delta - \arctan\left(\frac{v_y + \dot{\psi}l_f}{v_x}\right)\right) - I_z\ddot{\psi}\Bigg] - v_x\dot{\psi} \quad (31)$$

Where $b = \frac{l\cos\delta}{ml_r}\left(\frac{\mu_{f,l}}{s_{f,l}}\ F_{z_{f,l}} + \frac{\mu_{f,r}}{s_{f,r}}\ F_{z_{f,r}}\right)$. On the other hand, using "Eq. (24)", $\dot{v}_y$ can be written as:

$$\dot{v}_y = \dot{v}_{y_c} + K_{v_y}e_{v_y} + K_{i,v_y}\int_0^t e_{v_y}\,dt \quad (32)$$

By setting the right side of "Eq. (31) and Eq. (32)" equal, the steering angle δ can be determined as:

$$\delta = \frac{1}{b}\Bigg[\frac{ml_r}{l}\left(\dot{v}_{y_c} + K_{v_y}e_{v_y} + K_{i,v_y}\int_0^t e_{v_y}\,dt + v_x\dot{\psi}\right) - F_{x_f}\sin\delta_{-1} + I_z\ddot{\psi}\Bigg] + \arctan\left(\frac{v_y + \dot{\psi}l_f}{v_x}\right) \quad (33)$$

4 ONLINE ESTIMATION ALGORITHM OF TIRE FORCES AND TIRE-ROAD FRICTION COEFFICIENTS

It can be seen carefully in "Eq. (28), Eq. (29), and (33)" that the tire forces must also be known to calculate the control inputs. Since the complex dynamics of tires depend on environmental changes, tire wear, and unpredictable road conditions, the online estimation of these forces is necessary. In references [40-44], methods of identifying parameters of complex tire models, friction coefficient, and tire forces have been reviewed. Generally, past research in this field can be classified into cause-based and effect-based estimation methods. The concentration of cause-based methods is on studying and diagnosing effective factors in the tire-road interaction, and the friction coefficient is identified using specific analytical theories [43]. Effect-based techniques also use vehicle response to determine the friction coefficient [44].

In this research, according to the concept of friction circle and the use of vehicle kinematic characteristics that can be measured or estimated by sensors, tire forces, and friction coefficients are computed online with a straightforward algebraic algorithm and updated in the control law.

Since the proposed method works based on the vehicle response, it is an effect-based estimation technique. The details of the proposed method are presented below.

4.1. Calculation of The Longitudinal and Lateral Tire Forces

For simplicity, the vehicle's motion Equations are first rewritten in the following form:

$$ma_x = F_{x_f}\cos\delta - F_{y_f}\sin\delta + F_{x_r} - F_{aero} \quad (34)$$

$$ma_y = F_{x_f}\sin\delta + F_{y_f}\cos\delta + F_{y_r} \quad (35)$$

$$ma_y = F_{x_f}\sin\delta + F_{y_f}\cos\delta + F_{y_r} \quad (36)$$

Now, we multiply both sides of "Eq. (35)" by $(-l_f)$ and add both sides of the resulting Equation with Eq. (36) to obtain "Eq. (37)".

$$F_{y_r} = \frac{l_f ma_y - I_z\ddot{\psi}}{l} \quad (37)$$

Knowing a_y and $\ddot{\psi}$ then F_{y_r} can be calculated. According to "Eq. (34) and Eq. (35)", to calculate F_{y_f}, the longitudinal forces of the tires must be determined first. Besides, because the distribution of traction and braking torques are unlike, $F_{x_f}$and F_{x_r} are also different for braking and traction modes. Therefore, these two states are separated from each other in the following.

4.1.1. Traction Mode

For front-wheel drive vehicles, F_{x_f} can be computed from the wheel dynamic "Eq. (13)".

$$F_{x_r} = \frac{I_w}{r_w}\left(\dot{\omega}_{r,l} + \dot{\omega}_{r,r}\right) + f_r F_{z_r} \quad (38)$$

Considering that the values of F_{x_r} and F_{y_r} have been determined to calculate F_{x_f} and F_{y_f} both sides of "Eq. (34) and Eq. (35)" are multiplied by $\cos\delta$ and $\sin\delta$, respectively, and next, the sum of the sides of two Equations yields:

$$m\left(a_x\cos\delta + a_y\sin\delta\right) = F_{x_f} + \left(F_{x_r} - F_{aero}\right)\cos\delta + F_{y_r}\sin\delta \quad (39)$$

By replacing the equivalent terms for F_{y_r} and F_{x_r} from "Eq. (37) and Eq. (38)" in "Eq. (39)", the value of F_{x_f} can be determined as:

$$F_{x_f} = \left(ma_x + F_{aero} - \frac{I_w \dot{\omega}_r}{r_w} - f_r F_{z_r}\right)\cos\delta + \left(ma_y + \frac{I_z \ddot{\psi} - l_f m a_y}{l}\right)\sin\delta \quad (40)$$

Finally, by replacing the equivalent terms for F_{x_f} and F_{y_r} from "Eq. (40) and Eq. (37)" in "Eq. (35)", the value of F_{y_f} will be obtained as:

$$F_{y_f} = \frac{ma_y - F_{x_f}\sin\delta - F_{y_r}}{\cos\delta} \quad (41)$$

4.1.2. Braking Mode

Considering the traditional braking torque distribution strategy, "Eq. (34)" can be written as:

$$ma_x = (\gamma + \cos\delta)F_{x_f} - F_{y_f}\sin\delta - F_{aero} \quad (42)$$

Now multiplying the sides of "Eq. (35) and Eq. (42)" by $\sin\delta$ and $\cos\delta$, respectively, and then adding the two sides of the resulting Equations together yields:

$$m(a_x\cos\delta + a_y\sin\delta) = (\gamma\cos\delta + 1)F_{x_f} - F_{aero}\cos\delta + F_{y_r}\sin\delta \quad (43)$$

By replacing F_{y_r} from "Eq. (37)" in "Eq. (43)" and making appropriate simplifications for F_{x_f}, the "Eq. (44)" will be obtained as:

$$F_{x_f} = \left[\frac{(ma_x + F_{aero})\cos\delta + \left(\frac{I_z\ddot{\psi} + l_r m a_y}{l}\right)\sin\delta}{(\gamma\cos\delta + 1)}\right] \quad (44)$$

By replacing the equivalent terms for F_{x_f} and F_{y_r} from (45) and (37) in "Eq. (41)", the value of F_{y_f} can be determined. Until this stage, the values of F_{x_f}, F_{x_r}, F_{y_f}, F_{y_r} have been determined.

4.2. Calculation of Tire Friction Coefficients

According to "Eq. (28), Eq. (29), and (33)", it can be seen that it is not necessary to calculate the tire-road friction coefficients to determine the control inputs at any moment. However, to check the accuracy of the considered tire model and to evaluate the method of estimating the longitudinal and lateral forces of the tire, in this section, the method of calculating the friction coefficient of front axle tires ($\mu_{f,l}$ and $\mu_{f,r}$) will be explained. Similarly, the friction coefficient values of rear axle tires ($\mu_{r,l}$ and $\mu_{r,r}$) can be calculated. To calculate the friction coefficient of the front axle tires ($\mu_{f,l}$ and $\mu_{f,r}$), the longitudinal and lateral forces of each of the front axle tires should be calculated. In the dynamic model section, it was stated that for each axis, the longitudinal forces of the left and right tires are almost equal.

$$F_{x_{\tau,l}} \approx F_{x_{\tau,r}} \approx \frac{F_{x_\tau}}{2}, \quad \tau \in \{f, r\} \quad (45)$$

Using "Eq. (5), Eq. (11), and Eq. (47)" for the front tires, we have:

$$\frac{F_{x_f}}{2} = \sigma_{x_{f,l}}\frac{\mu_{f,l}}{\sigma_{f,l}}F_{z_{f,l}} \quad (46)$$

$$\frac{F_{x_f}}{2} = \sigma_{x_{f,r}}\frac{\mu_{f,r}}{\sigma_{f,r}}F_{z_{f,r}} \quad (47)$$

$$F_{y_{f,l}} = \sigma_{y_f}\frac{\mu_{f,l}}{\sigma_{f,l}}F_{z_{f,l}} \quad (48)$$

$$F_{y_{f,r}} = \sigma_{y_f}\frac{\mu_{f,r}}{\sigma_{f,r}}F_{z_{f,r}} \quad (49)$$

By dividing both sides of "Eq. (47)" by "Eq. (48)" and dividing "Eq. (49)" by "Eq. (50)", "Eq. (51) and Eq. (52)" will be obtained, respectively.

$$\frac{\sigma_{x_{f,r}}}{\sigma_{x_{f,l}}} = \frac{\sigma_{f,r}}{\sigma_{f,l}}\frac{\mu_{f,l}}{\mu_{f,r}}\frac{F_{z_{f,l}}}{F_{z_{f,r}}} \quad (50)$$

$$\frac{F_{y_{f,l}}}{F_{y_{f,r}}} = \frac{\sigma_{f,r}}{\sigma_{f,l}}\frac{\mu_{f,l}}{\mu_{f,r}}\frac{F_{z_{f,l}}}{F_{z_{f,r}}} \quad (51)$$

By combining "Eq. (51) and Eq. (52)", between the lateral force of the front tires, "Eq. (53)" is obtained.

$$\frac{F_{y_{f,l}}}{F_{y_{f,r}}} = \frac{\sigma_{x_{f,r}}}{\sigma_{x_{f,l}}} \quad (52)$$

Considering that the value of F_{y_f} is known, the lateral force of each of these tires can be calculated using "Eq. (53)". By determining the normal force, longitudinal force, and lateral force of each of the front tires, the approximate value of the tire-road friction coefficient of each of these tires can be calculated as:

$$\mu_{f,\varepsilon} = \frac{\sqrt{\left(F_{x_{f,\varepsilon}}\right)^2 + \left(F_{y_{f,\varepsilon}}\right)^2}}{F_{z_{f,\varepsilon}}}, \quad \varepsilon \in \{l, r\} \tag{53}$$

5 OBTAINED RESULTS

To evaluate the effectiveness of the proposed adaptive control, CarSim and MATLAB/Simulink software packages have been used. The dynamic model used for simulation has 14 degrees of freedom to include the dynamics of the suspension system, brake system, power chain, steering system, and the dynamics of the steering wheel actuator. Pacejka 5.2 (Symmetric) tire model is also used for tires. The vehicle used in the simulations is a typical D-class sedan with default parameters from CarSim database.

The block diagram of longitudinal-lateral adaptive integrated control is shown in Fig. 3. To evaluate the performance of the control algorithm in conditions closer to reality, the Vehicle State Calculation block is considered. This block is responsible for estimating the speed, filtering the noise of the sensors, and calculating some vehicle states. In this simulation, it is presumed that longitudinal acceleration, lateral acceleration, and steering angle rate are measured by IMU and have noise. To consider the effect of noise, the Band-Limited White Noise block of Simulink is used. It is also assumed that the coordinates of the vehicle CG, wheel speed, and gear ratio are accessible. The considered noise power value for $\dot{\psi}$, a_x and a_y is equal to 0.001 deg/sec, $0.5 \times 10^{-6} g$ and $10^{-6} g$, respectively. A 1st order low-pass Butterworth filter with a pass frequency of 10 Hz was used for filtering. For the steering wheel angle, the saturation limit is ±10 deg. In the simulation, the steering wheel angular position actuator's dynamics is also considered a second-order transfer function with a natural frequency of 6.3 Hz and damping of 0.95 [45]. The reference method [30] has also been used to estimate longitudinal and lateral velocities.

To evaluate the performance of the integrated control proposed in this section, three different maneuvers have been planned, including moving on a curved road, the critical lane change in braking mode, and the critical lane change in traction mode. In the following, the details of the obtained results of these scenarios are described in detail.

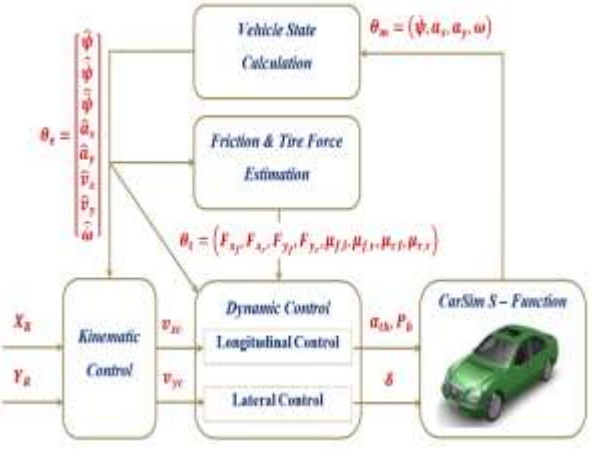

Fig. 3 Block diagram of integrated longitudinal and lateral control.

5.1. Maneuver I: Constant Speed on A Curved Road

In this maneuver, the vehicle speed is assumed to be constant and equal to 36 km/h. Figure 4a shows the desired path and the direction of the vehicle. With a general look, it can be said that the desired path of the vehicle has been followed with appropriate accuracy. In order to investigate the tracking more precisely, the longitudinal and lateral tracking errors are shown in "Fig. 4c and Fig. 4d", respectively. According to these figures, it can be seen that the maximum of longitudinal and lateral tracking errors is insignificant and is around 0.4 m. In the part with the curved path, as expected, the steering angle of the wheel is almost constant and its value is equal to 1.6 deg ("Fig. 4-b"). Considering the constant speed during the maneuver, it is expected that the amount of throttle opening and the torque applied to the wheels will be constant. Examining "Fig. 4e and Fig. 4f" confirms this point well. The amount of throttle opening is 10%, and the amount of torque applied to each front wheel is 20 N.m.

5.2. Maneuver Ii: Lane Change with Braking

This maneuver is planned to evaluate the integrated control performance in high-speed braking maneuvers. The vehicle's initial speed is assumed to be 140 km/h. It is assumed that the vehicle first moves for 3 seconds with a constant braking acceleration of -2.5 m/sec^2 and then changes lanes with the same braking acceleration. After the lane change, the vehicle continues to move with the same acceleration for 10 seconds ("Fig. 5").

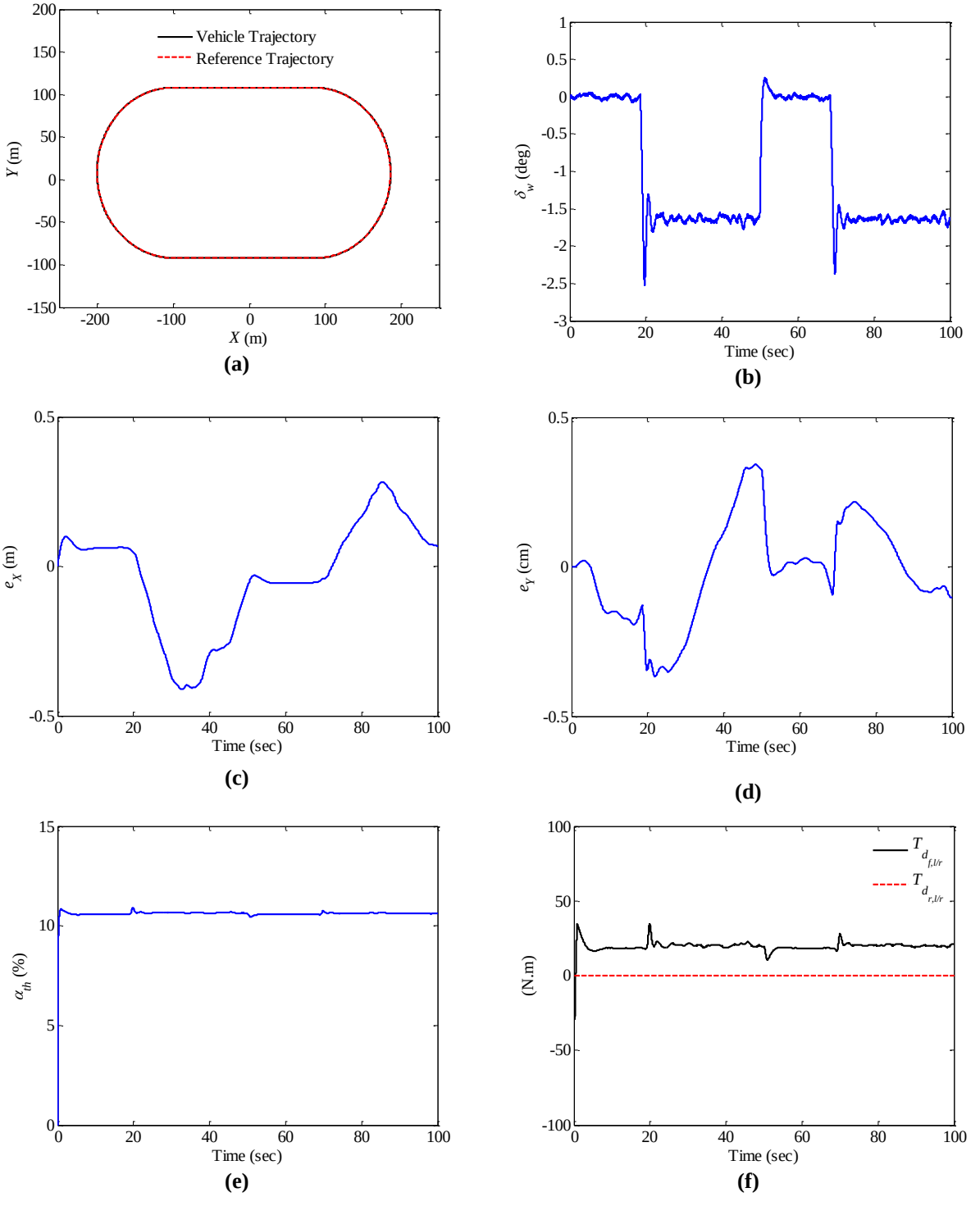

Fig. 4 Integrated control performance in the curved path: (a): reference path and vehicle path, (b): steering wheel angle, (c): longitudinal tracking error, (d): lateral tracking error, (e): throttle opening percentage, and (f): traction torque applied to the wheels.

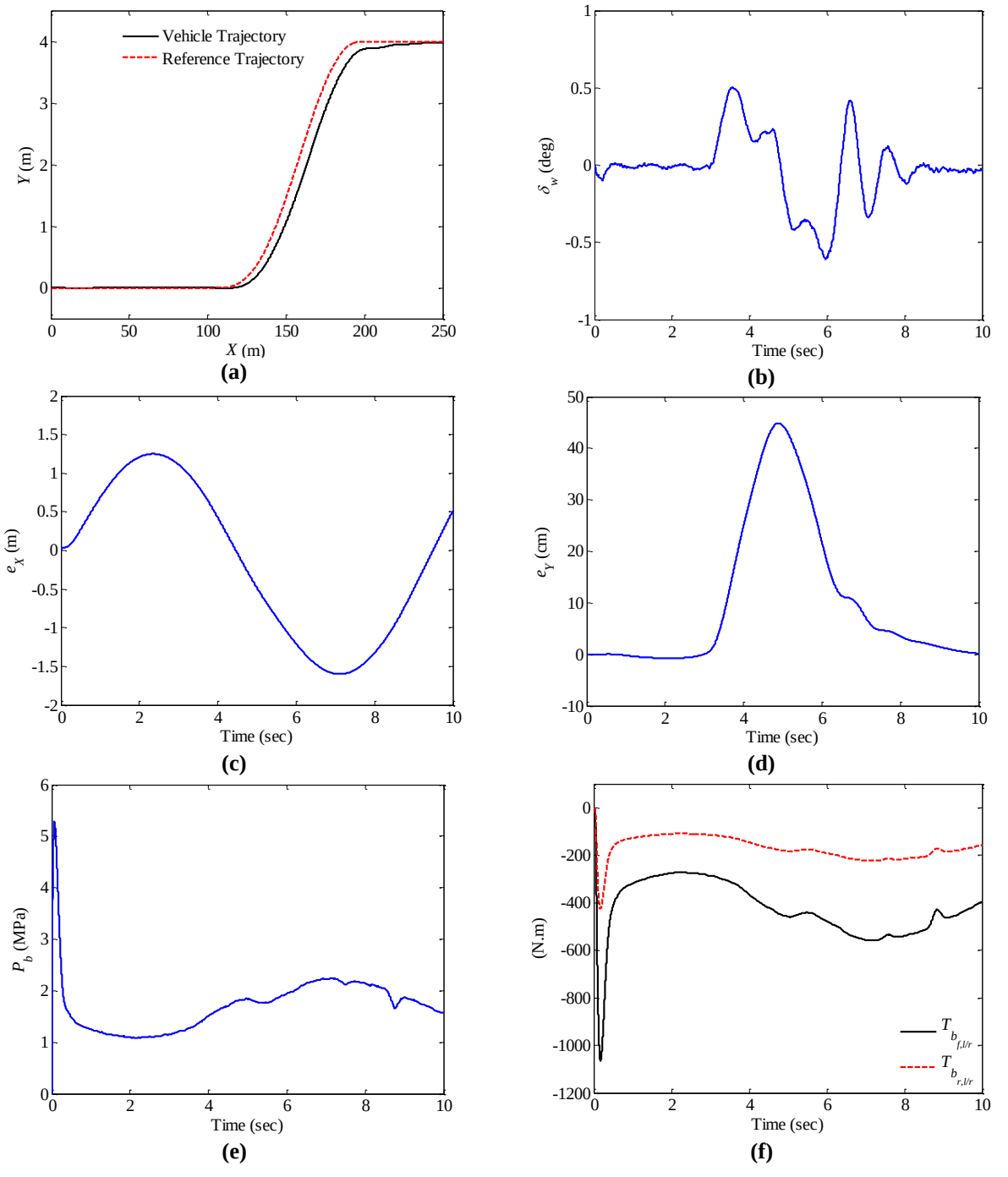

Fig. 5 Integrated control performance in braking lane change: (a): reference path and vehicle path, (b): steering wheel angle, (c): longitudinal tracking error, (d): lateral tracking error, (e): master cylinder brake pressure, and (f): braking torque

5.3. Maneuver Iii: Lane Change with Accelerating

The characteristics of the maneuver are shown in "Fig. 6 and Fig. 7a". This maneuver includes two lane changes, the first lane change is done with a constant acceleration of 1.5 m/sec^2, and the second lane change is done with a constant speed. The changes in the maximum available tire-road friction coefficient ($\mu_{ro,max}$) in terms of the longitudinal position of the road are presented in "Fig. 6a". In the middle of the first lane change (150 m to 155 m), $\mu_{ro,max}$ changes from 0.9 to 0.7. Also, In the middle

of the second lane change (410 m to 415 m), $\mu_{ro,max}$ decreases from 0.7 to 0.4. The initial speed of the vehicle is 100 km/h.

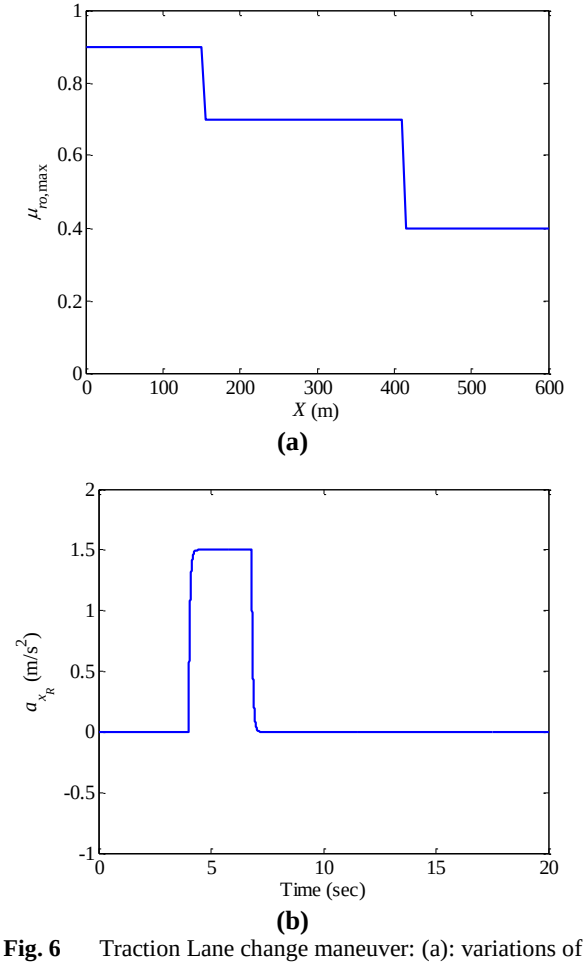

Fig. 6 Traction Lane change maneuver: (a): variations of road friction coefficient, and (b): reference longitudinal acceleration.

The vehicle motion path and tracking errors are shown in "Fig. 7". It can be seen in this figure that the desired motion path has been followed well and with little error. The maximum longitudinal tracking error is less than 1 m ("Fig. 7b"), and the maximum lateral tracking error is less than 30 cm ("Fig. 7c").

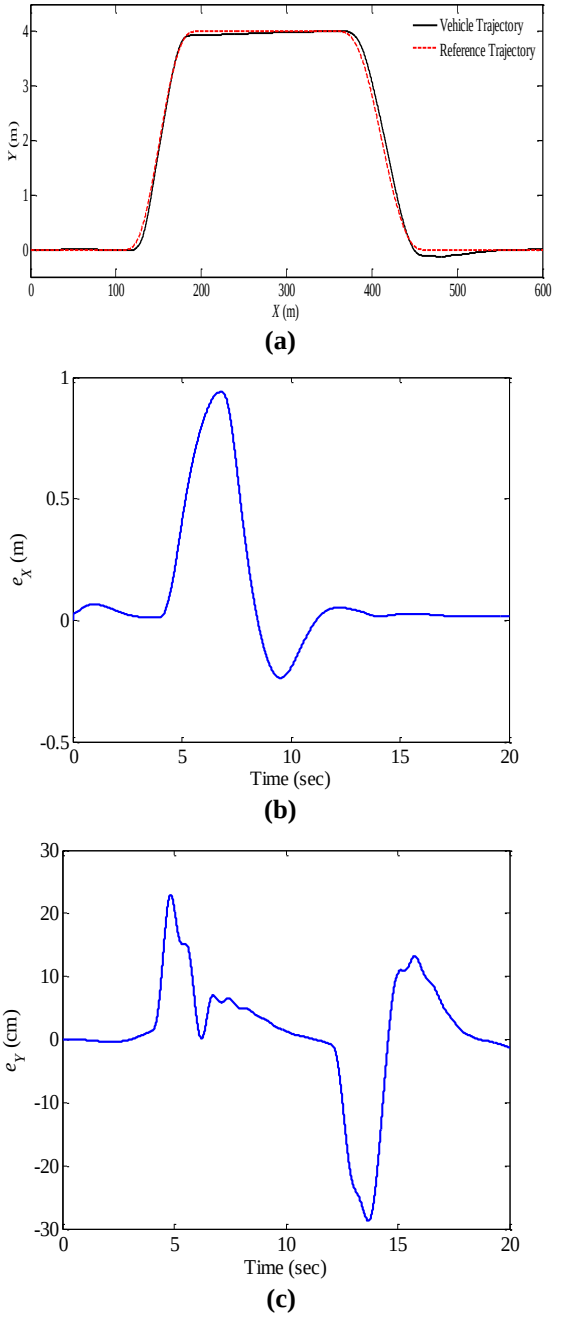

Fig. 7 The complete performance of the integrated control in lane change: (a): reference path and vehicle path, (b): longitudinal tracking error, and (c): lateral tracking error.

The longitudinal and lateral control inputs are also shown in "Fig. 8a and Fig. 8b", respectively.

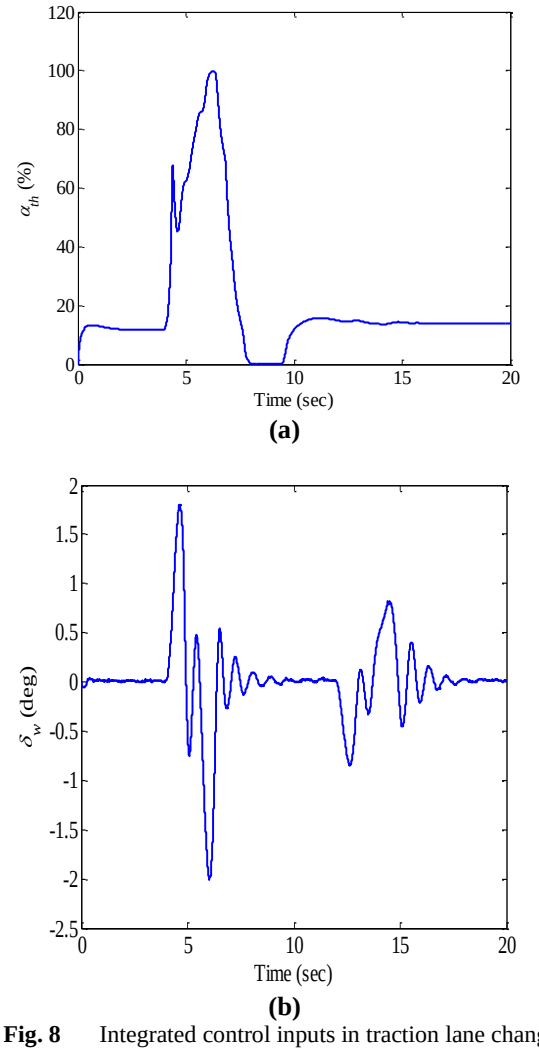

Fig. 8 Integrated control inputs in traction lane change: (a): Throttle valve opening percentage, and (b): Wheel steering angle.

In order to assess the changes in the longitudinal and lateral speed variations and the accuracy of the speed estimation, the longitudinal and lateral speeds of the vehicle, along with their estimated values, are shown in "Fig. 9a and Fig. 9b", respectively.

Finally, car friction coefficients and their estimated values are presented in "Fig. 10." The accuracy of the tire friction coefficient estimation can be assessed by examining "Fig. 10". In "Fig. 10b", it can be observed that the friction coefficient of the tire reaches its maximum available value of 0.7 within 6.2 seconds. This indicates that the tire has reached its maximum frictional capacity at this point in time. Considering this finding, it can be concluded that the proposed integrated adaptive control strategy is capable of performing its task effectively and following the desired path with acceptable accuracy, even under critical driving conditions involving changes in road friction and tire dynamic nonlinearities.

One of the key advantages of the proposed control approach is its robustness. The controller was designed based on a 7-degree-of-freedom vehicle model, yet the simulations were conducted using the full vehicle dynamic model. This suggests that the presented control strategy has successfully accounted for various parametric and unmodeled uncertainties, demonstrating its ability to handle the complexity of the actual vehicle dynamics. Furthermore, the ability of the control system to fully utilize the tire's maximum frictional capacity, as evident from the friction coefficient reaching 0.7, implies that the control strategy is effectively managing the available tire-road adhesion.

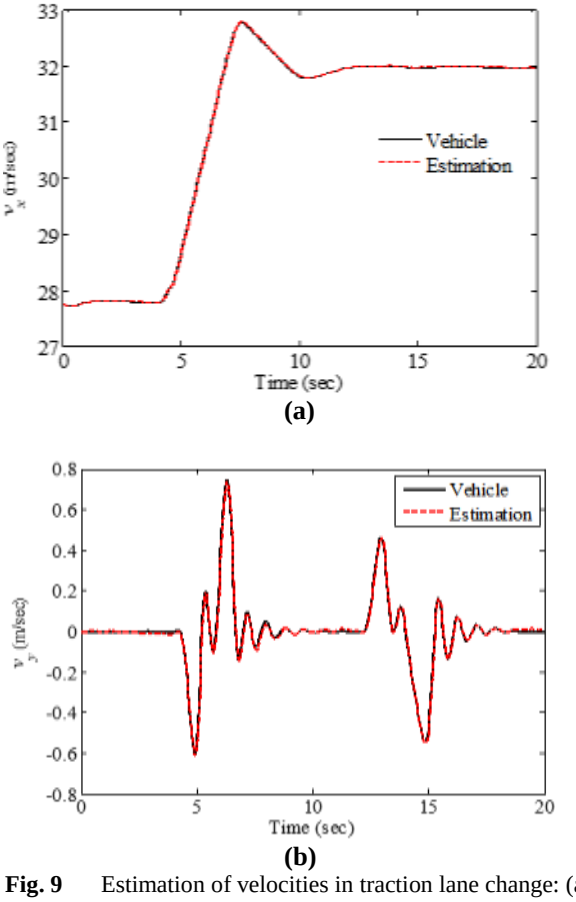

Fig. 9 Estimation of velocities in traction lane change: (a): longitudinal speed, and (b): lateral speed.

This is a crucial aspect, especially in critical driving scenarios where the vehicle's performance and stability are heavily dependent on the optimal utilization of the tire-road interface. By combining the accurate estimation of the tire friction coefficient, the effective handling of tire dynamic nonlinearities, and the demonstrated robustness against uncertainties, the proposed integrated adaptive control approach shows promise in maintaining the vehicle's desired path-tracking performance and stability, even in challenging driving conditions characterized by changes in road

friction and other nonlinear vehicle dynamics.

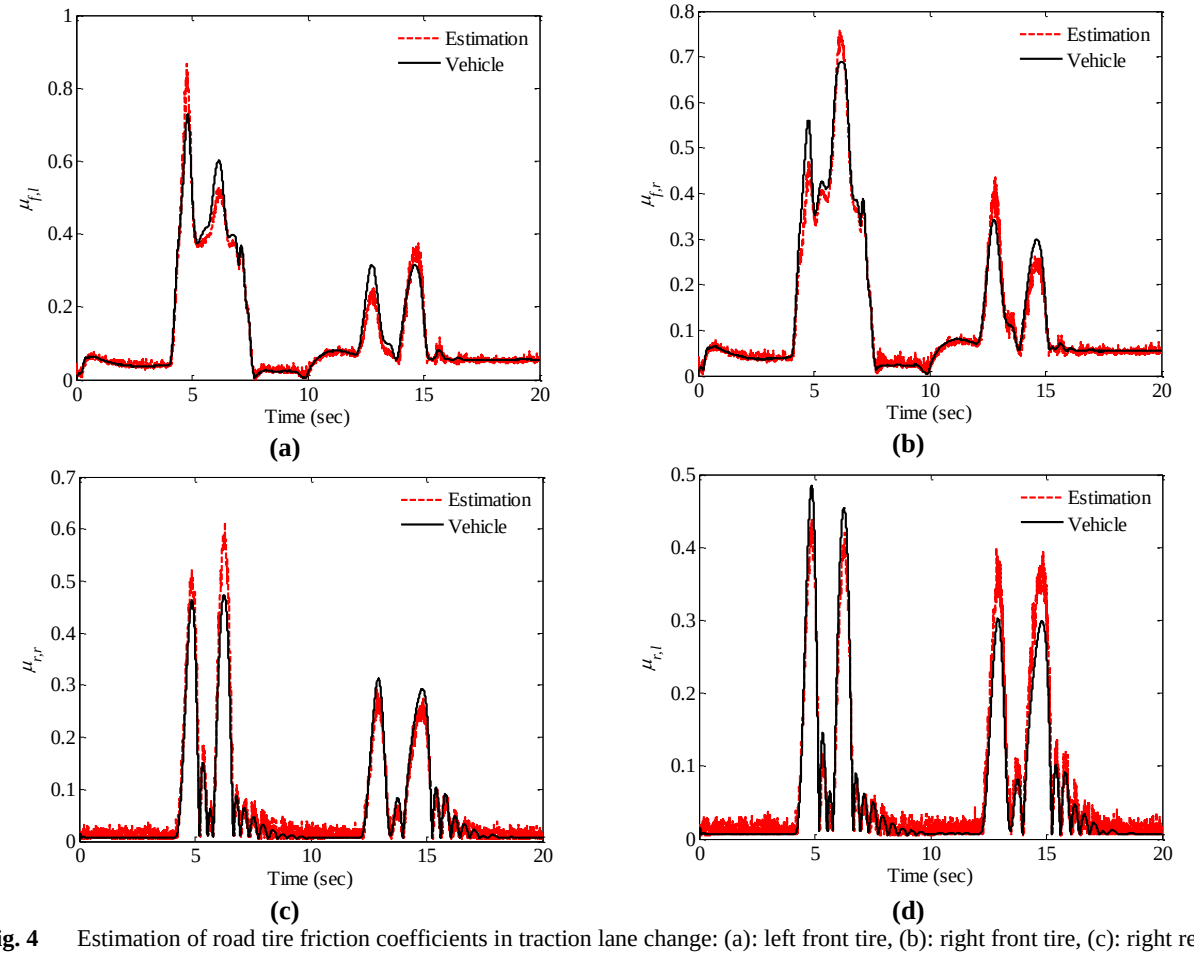

Fig. 4 Estimation of road tire friction coefficients in traction lane change: (a): left front tire, (b): right front tire, (c): right rear tire, and (d): left rear tire.

6 CONCLUSIONS

The proposed adaptive control algorithm represents a significant advancement in managing highly nonlinear vehicle dynamics and sudden changes in friction coefficients. This control strategy has substantial potential for real-world driving applications. The key practical implications include the controller's robustness to accommodate changes in friction coefficient and other uncertainties, as well as its capability to accurately track curved paths. These features are critical for enhancing driving safety and control, especially in challenging road conditions or when integrated with advanced driver assistance systems. The simulation results demonstrate the effectiveness of the integrated adaptive control in managing complex maneuvers, such as constant-speed cornering, lane changes under braking, and lane changes under traction. These findings suggest the controller could be successfully implemented in real-world vehicles, providing enhanced stability and performance. Furthermore, the accurate estimation of the friction coefficient underscores the potential for this control approach to contribute to advanced tire-road interaction models and friction estimation algorithms, with far-reaching implications for vehicle safety and performance systems. For future work, it is recommended to evaluate the controller's performance when integrated with electronic stability control (ESC), as well as to validate the simulation results through extensive testing on physical prototypes. Exploring the controller's behavior under extreme conditions, such as split-μ scenarios, and investigating the potential for incorporating machine learning techniques could further enhance the controller's adaptability and robustness. By addressing these future research directions, the practical applicability and impact of the proposed adaptive control algorithm can be expanded, paving the way for its widespread adoption in real-world vehicle applications.

REFERENCES

[1] Thorpe, C., Herbert, M., Kanade, T., and Shafter, S., Toward Autonomous Driving: the CMU Navlab, II. Architecture and Systems, IEEE Expert, Vol. 6, No. 4, pp. 44-52, 1991, doi: 10.1109/64.85920.

[2] Dickmanns E. D., Zapp, A., Autonomous High Speed Road Vehicle Guidance by Computer Vision1, IFAC Proceedings Volumes, Vol. 20, No. 5, Part. 4, pp. 221-226, 1987/07/01/ 1987, doi: https://doi.org/10.1016/S1474-6670(17)55320-3.

[3] Ni, J., Hu, J., and Xiang, C., A Review for Design and Dynamics Control of Unmanned Ground Vehicle, Proceedings of the Institution of Mechanical Engineers, Part D: Journal of Automobile Engineering, Vol. 235, No. 4, pp. 1084-1100, 2021, doi: 10.1177/0954407020912097.

[4] Road Traffic Injuries, https://www.who.int/news-room/fact-sheets/detail/road-traffic-injuries accessed.

[5] Administration, N. H. T. S., Motor Vehicle Crashes: Overview, Traffic Safety Facts: Research Note, Vol. 2016, 2016, pp. 1-9.

[6] You, F., Zhang, R., Lie, G., Wang, H., Wen, H., and Xu, J., Trajectory Planning and Tracking Control for Autonomous Lane Change Maneuver Based on The Cooperative Vehicle Infrastructure System, Expert Systems with Applications, Vol. 42, No. 14, pp. 5932-5946, 2015.

[7] Dixit S., et al., Trajectory Planning and Tracking for Autonomous Overtaking: State-of-The-Art and Future Prospects, Annual Reviews in Control, Vol. 45, pp. 76-86, 2018/01/01/ 2018, doi: https://doi.org/10.1016/j.arcontrol.2018.02.001.

[8] Wang, L., Zhao, X., Su, H., and Tang, G., Lane Changing Trajectory Planning and Tracking Control for Intelligent Vehicle on Curved Road, SpringerPlus, Vol. 5, No. 1, 2016, pp. 1150.

[9] Kayacan, E., Ramon, H., and Saeys, W., Robust Trajectory Tracking Error Model-Based Predictive Control for Unmanned Ground Vehicles, IEEE/ASME Transactions on Mechatronics, Vol. 21, No. 2, 2016, pp. 806-814, doi: 10.1109/TMECH.2015.2492984.

[10] Petrov P., Nashashibi, F., Modeling and Nonlinear Adaptive Control for Autonomous Vehicle Overtaking, IEEE Transactions on Intelligent Transportation Systems, Vol. 15, No. 4, pp. 1643-1656, 2014, doi: 10.1109/TITS.2014.2303995.

[11] Wnag, C., Zhao, W., Xu, Z., and Zhou, G., Path Planning and Stability Control of Collision Avoidance System Based on Active Front Steering, Science China Technological Sciences, Vol. 60, No. 8, pp. 1231-1243, 2017.

[12] Rasekhipour, Y., Khajepour, A., Chen, S. K., and Litkouhi, B., A Potential Field-Based Model Predictive Path-Planning Controller for Autonomous Road Vehicles, IEEE Transactions on Intelligent Transportation Systems, Vol. 18, No. 5, pp. 1255-1267, 2016.

[13] Suh, J., Chae, H., and Yi, K., Stochastic Model-Predictive Control for Lane Change Decision of Automated Driving Vehicles, IEEE Transactions on Vehicular Technology, Vol. 67, No. 6, pp. 4771-4782, 2018, doi: 10.1109/TVT.2018.2804891.

[14] Cai, J., Jiang, H., Chen, L., Liu, J., Cai, Y., and Wang, J., Implementation and Development of a Trajectory Tracking Control System for Intelligent Vehicle, Journal of Intelligent & Robotic Systems, 2018/05/09 2018, doi: 10.1007/s10846-018-0834-4.

[15] Feng, P., Jin, H., Zhao, L., and Lu, M., Active Lane-Changing Control of Intelligent Vehicle on Curved Section of Expressway, Modelling and Simulation in Engineering, Vol. 2022, 2022.

[16] Xiong, L., Yang, X., Leng, B., Zhang, R., Fu, Z., and Zhuo, G., Integrated longitudinal and lateral control for autonomous vehicles with active load transfer strategy at the handling limits, Proceedings of the Institution of Mechanical Engineers, Part D: Journal of Automobile Engineering, Vol. 235, No. 4, 2021, pp. 961-974.

[17] Wang, H., Zhang, T., Zhang, X., and Li, Q., Observer-Based Path Tracking Controller Design for Autonomous Ground Vehicles with Input Saturation, IEEE/CAA Journal of Automatica Sinica, Vol. 9, 2022, pp. 1-13.

[18] Hossain, T., Habibullah, H., and Islam, R., Steering and Speed Control System Design for Autonomous Vehicles by Developing an Optimal Hybrid Controller to Track Reference Trajectory, Machines, Vol. 10, No. 6, 2022, pp. 420.

[19] Guo, J., Hu, P., and Wang, R., Nonlinear Coordinated Steering and Braking Control of Vision-Based Autonomous Vehicles in Emergency Obstacle Avoidance, IEEE Transactions on Intelligent Transportation Systems, Vol. 17, No. 11, 2016, pp. 3230-3240, doi: 10.1109/TITS.2016.2544791.

[20] Choi, J., Yi, K., Suh, J., and Ko, B., Coordinated Control of Motor-Driven Power Steering Torque Overlay and Differential Braking for Emergency Driving Support, IEEE Transactions on Vehicular Technology, Vol. 63, No. 2, 2014, pp. 566-579, doi: 10.1109/TVT.2013.2279719.

[21] Funke, J., Brown, M., Erlien, S. M., and Gerdes, J. C., Collision Avoidance and Stabilization for Autonomous Vehicles in Emergency Scenarios, IEEE Transactions on Control Systems Technology, Vol. 25, No. 4, 2017, pp. 1204-1216, doi: 10.1109/TCST.2016.2599783.

[22] Song, J., Development and Comparison of Integrated Dynamics Control Systems with Fuzzy Logic Control and Sliding Mode Control, J. Mech Sci Technol, Vol. 27, No. 6, 2013, pp. 1853-1861.

[23] Zhang, Z., Wang, C., Zhao, W., and Feng, J., Longitudinal and Lateral Collision Avoidance Control Strategy for Intelligent Vehicles, Proceedings of the Institution of Mechanical Engineers, Part D: Journal of

Automobile Engineering, 2022, pp. 09544070211024048.

[24] Chen, R., Chen, Z., Duan, Y., Wu, DJ., and Zhang, Y., Coupled Longitudinal and Lateral Control for Trajectory Tracking of Autonomous Vehicle Based on LTV-MPC Approach, SAE Technical Paper, 0148-7191, 2022.

[25] Li, Z., Chen, Liu, H., Wang, P., and Gong, X., Integrated Longitudinal and Lateral Vehicle Stability Control for Extreme Conditions With Safety Dynamic Requirements Analysis, IEEE Transactions on Intelligent Transportation Systems, 2022.

[26] Li, Z., Wang, P., Cai, S., Hu, X., and Chen, H., NMPC-Based Controller for Vehicle Longitudinal and Lateral Stability Enhancement Under Extreme Driving Conditions, ISA Transactions, Vol. 135, 2023, pp. 509-523.

[27] Attia, R., Orjuela, R., and Basset, M., Combined Longitudinal and Lateral Control for Automated Vehicle Guidance, Vehicle System Dynamics, Vol. 52, No. 2, 2014, pp. 261-279, doi: 10.1080/00423114.2013.874563.

[28] Liu, Y., Pei, Guo X., Chen, C., and Zhou, H., An Integration Planning and Control Method of Intelligent Vehicles Based on The Iterative Linear Quadratic Regulator, Journal of the Franklin Institute, Vol. 361, No. 1, 2024, pp. 265-282.

[29] Jin, X., Wang, Q., Yan, Z., Yang, H., and Yin, G., Integrated Robust Control of Path Following and Lateral Stability for Autonomous in-Wheel-Motor-Driven Electric Vehicles, Proceedings of the Institution of Mechanical Engineers, Part D: Journal of Automobile Engineering, 2024, pp. 09544070241227266.

[30] Sazgar, H., Azadi, S., and Kazemi, R., and Khalaji, A. K., Integrated Longitudinal and Lateral Guidance of Vehicles in Critical High Speed Maneuvers, Proceedings of the Institution of Mechanical Engineers, Part K: Journal of Multi-body Dynamics, Vol. 233, No. 4, 2019, pp. 994-1013, doi: 10.1177/1464419319847916.

[31] Sazgar, H., Azadi, S., and Kazemi, R., Trajectory Planning and Combined Control Design for Critical High-Speed Lane Change Maneuvers, Proceedings of the Institution of Mechanical Engineers, Part D: Journal of Automobile Engineering, Vol. 234, No. 2-3, 2020, pp. 823-839, doi: 10.1177/0954407019845253.

[32] Sazgar, H., Khalaji, A. K., Nonlinear Integrated Control with Friction Estimation for Automatic Lane Change on The Highways, Proceedings of the Institution of Mechanical Engineers, Part K: Journal of Multi-body Dynamics, Vol. 236, No. 3, 2022, pp. 453-469.

[33] Rajamani, R., Vehicle Dynamics and Control. Springer Science & Business Media, 2011.

[34] Kiencke, U., Nielsen, L., Automotive Control Systems: for Engine, Driveline, and Vehicle, ed: IOP Publishing, 2000.

[35] Pacejka H., Besselink, I., Tire, and Vehicle Dynamics. Elsevier Science, 2012.

[36] Hwan J. J., et al., Optimal Motion Planning with the Half-Car Dynamical Model for Autonomous High-Speed Driving, in 2013 American Control Conference, Vol. 17-19, 2013, pp. 188-193, doi: 10.1109/ACC.2013.6579835.

[37] Velenis, E., Tsiotras, P., and Lu, J., Optimality Properties and Driver Input Parameterization for Trail-Braking Cornering, European Journal of Control, Vol. 14, No. 4, 2008, pp. 308-320.

[38] Bakker, E., Nyborg, L., and Pacejka, H. B., Tyre Modelling for Use in Vehicle Dynamics Studies, 1987. [Online], Available: https://doi.org/10.4271/870421.

[39] Milanés, V., González, C., Naranjo, J., Onieva, E., and De Pedro, T., Electro-Hydraulic Braking System for Autonomous Vehicles, International Journal of Automotive Technology, Vol. 11, No. 1, 2010, pp. 89-95.

[40] Khaleghian, S., Emami, A., and Taheri, S., A Technical Survey on Tire-Road Friction Estimation, Friction, Vol. 5, No. 2, 2017, pp. 123-146.

[41] Singh, K. B., Arat, M. A., and Taheri, S., Literature Review and Fundamental Approaches for Vehicle and Tire State Estimation, Vehicle System Dynamics, 2018, pp. 1-23.

[42] Guo, H., Yin, Z., Cao, D., Chen, H., and Lv, C., A Review of Estimation for Vehicle Tire-Road Interactions Toward Automated Driving, IEEE Transactions on Systems, Man, and Cybernetics: Systems, No. 99, 2018, pp. 1-17.

[43] Peng, Y., Chen, J., and Ma, Y., Observer-Based Estimation of Velocity and Tire-Road Friction Coefficient for Vehicle Control Systems, Nonlinear Dynamics, Journal article, Vol. 96, No. 1, 2019, pp. 363-387, doi: 10.1007/s11071-019-04794-0.

[44] Beal, C. E., Rapid Road Friction Estimation using Independent Left/Right Steering Torque Measurements, Vehicle System Dynamics, 2019, pp. 1-27, doi: 10.1080/00423114.2019.1580377.

[45] Cerone, V., Milanese, M., and D. Regruto, Combined Automatic Lane-Keeping and Driver's Steering through a 2-DOF Control Strategy, IEEE Transactions on Control Systems Technology, Vol. 17, No. 1, 2008, pp. 135-142.